MEDICAL ROBOTS

An ingestible capsule for luminance-based diagnosis of mesenteric ischemia

J. Chen[1,2]†, A. Alexiev[2]†, A. Sergnese[2]†, N. Fabian[1,3,4], A. Pettinari[1], Y. Cai[5], V. Perepelook[1], K. Schmidt[1], A. Hayward[1,2,4], A. Guevara[4], B. Laidlaw[4], I. Moon[4], B. Markowitz[1], I. Ballinger[1], Z. Yang[1], C. Rosen[1,2], N. Shalabi[1,2], S. Owyang[2], G. Traverso[1,2,4,6]*

Acute mesenteric ischemia (AMI) results from insufficient blood flow to the intestines, leading to tissue necrosis with high morbidity and mortality. Diagnosis is often delayed because of nonspecific symptoms that mimic common gastrointestinal conditions. Current diagnostic methods, such as computed tomography and mesenteric angiography, are complex, costly, and invasive, highlighting the need for a rapid, accessible, and minimally invasive alternative. Here, we present FIREFLI (finding ischemia via reflectance of light), a bioinspired, ingestible capsule designed for luminance-based diagnosis of AMI. Upon ingestion, the device activates in the small intestine's pH environment, emitting pulses from three radially spaced white light-emitting diodes and measuring reflected light across 10 wavelengths. FIREFLI then computes a tissue luminance biomarker, which outperforms color-change biomarkers because of superior intrasubject consistency. The diagnosis is processed onboard and wirelessly transmitted to an external mobile device. In vivo studies in swine ($n = 9$) demonstrated a diagnostic accuracy of 90%, with a sensitivity of 98% and specificity of 85%. By providing a noninvasive, real-time diagnostic solution, FIREFLI has the potential to facilitate earlier detection and treatment of AMI, ultimately improving patient outcomes.

INTRODUCTION

Mesenteric ischemia is a gastrointestinal (GI) condition that arises from insufficient blood flow to the mesenteric arteries, leading to inadequate perfusion of the intestines. Mesenteric ischemia can present either acutely [acute mesenteric ischemia (AMI)] or chronically. AMI is particularly life threatening, with a short-term mortality of 55% (*1*), most commonly via bowel infarction, sepsis, and multiorgan failure (*2*).

Early detection of AMI and intervention are crucial for improving patient outcomes, but diagnosis remains challenging because of nonspecific symptoms and the need for high clinical suspicion. Patients often present with vague abdominal pain out of proportion with a physical exam, which can be mistaken for other, more common GI conditions (*3*, *4*), delaying diagnosis and treatment. (*5*).

Initially, patients may undergo numerous diagnostic studies (e.g., blood tests, abdominal x-rays, and computed tomography without arterial contrast) to evaluate for more common conditions, but these modalities are generally insufficient for the diagnosis of AMI. If there is a higher suspicion for AMI, then traditional diagnostic methods may be obtained, such as computed tomography angiography (CTA) or mesenteric angiography (*6*). These modalities may provide a diagnosis, but acquisition is often delayed, and such techniques may also confer the risk of radiation exposure and contrast-induced nephropathy. Additionally, interpretation of CTA requires expertise that may not be readily available, and mesenteric angiography is an invasive procedure requiring catheterization, specialized staff, and access to medical facilities. Diagnostic laparotomy is reserved for unstable patients or in cases where there is concern for advanced ischemia. As such, there is a need for more rapid, accessible, cost-effective, and minimally invasive diagnostic methods.

At this time, there is no specific biomarker for diagnosis of mesenteric ischemia (*7*). Although many have been proposed and studied, they may lack specificity, show conflicting results in clinical studies, or lack sufficient validation and are ultimately unable to provide reliable diagnoses in the early stages of disease (*8*). Thus, multiple studies have investigated methods to determine previously unidentified biomarkers (*9*) or predictors (*10*) to enable rapid, minimally invasive diagnosis.

An alternative paradigm for minimally invasive diagnosis of GI conditions is through the use of pill-sized ingestible electronic devices, which have unique access to a wide range of potential biomarkers, analytes, and signals (*11*). Video capsule endoscopy has detected ischemia (*12*) or consequences of ischemia (*13*) in some cases, but its efficacy has not been validated; limitations in field of view, frame rate, and illumination may result in low sensitivity and specificity (*14*). Although some improvements can be made (e.g., wider-angle lenses and brighter illumination), they do not fundamentally resolve the issue of real-time quantification of an ischemia biomarker with high specificity and selectivity. Previous works proposed ingestible gas sensors to detect gaseous GI biomarkers for inflammation such as hydrogen sulfide (*15*) or nitric oxide (NO) (*16*), with the NO biomarker showing promise in an in vivo swine model for ischemia. However, these sensors have many limitations, which may include high power consumption (*17*), vulnerability to moisture ingress (*16*), and limited specificity and selectivity resulting in cross-talk with other GI gases (*18*). Other works have proposed ingestible luminescent sensors that detect color to diagnose upper GI bleeding (*19*). Given that ischemic intestinal tissues display substantial color changes because of the lack of blood flow and oxygenation (*20*), this is a potential avenue for diagnosis for ingestible devices (*21*).

In this work, we propose an ingestible device for diagnosing this disease: FIREFLI (finding ischemia via reflectance of light). Inspired

[1]Department of Mechanical Engineering, Massachusetts Institute of Technology, Cambridge, MA, USA. [2]Division of Gastroenterology, Department of Medicine, Brigham and Women's Hospital, Harvard Medical School, Boston, MA, USA. [3]Division of Comparative Medicine, Massachusetts Institute of Technology, Cambridge, MA, USA. [4]Koch Institute for Integrative Cancer Research, Massachusetts Institute of Technology, Cambridge, MA, USA. [5]Program in Media Arts and Sciences, Massachusetts Institute of Technology, Cambridge, MA, USA. [6]Broad Institute of MIT and Harvard, Cambridge, MA, USA.
†These authors contributed equally to this work.
*Corresponding author. Email: cgt20@mit.edu

by the firefly, which emits light via pH-sensitive luciferase and detects light for orientation during mating, FIREFLI emits light after activation in the small intestine (SI) and detects light reflectance for orientation and disease diagnosis (Fig. 1, A to C, and fig. S1). The ingestible electronic capsule (11.0-mm diameter and 26.2-mm length) has a form factor similar to the PillCam SB 3 capsule used for capsule endoscopy (*22*). The device activates in the SI and operates with a 10% duty cycle to achieve a lifetime of 5.1 hours to enable diagnosis throughout SI transit. The electronic design comprises multiple stacking printed circuit boards (PCBs) for the microcontroller unit (MCU), antenna, logic level shifter, and sensing unit (Fig. 1B). The latter is a flexible PCB with three folding arms, each containing a white light-emitting diode (LED) and a 10-channel photodiode sensor. The electronics are powered by two Li-ion batteries and housed inside a biocompatible, three-dimensionally (3D) printed case. Cutouts in the case expose the LEDs and sensors, which are covered by a clear plastic film. The case and film are hermetically sealed using ultraviolet (UV)–cure epoxy.

The device was validated via in vivo experiments in a swine animal model, chosen because its GI anatomy is comparable to that of humans (*23*). In swine, mesenteric ischemia was induced by the well-documented method of clamping the mesenteric blood vessels (*24*–*26*). Using the tissue luminance biomarker, we demonstrated a diagnostic accuracy of 90% with a sensitivity of 98% and specificity

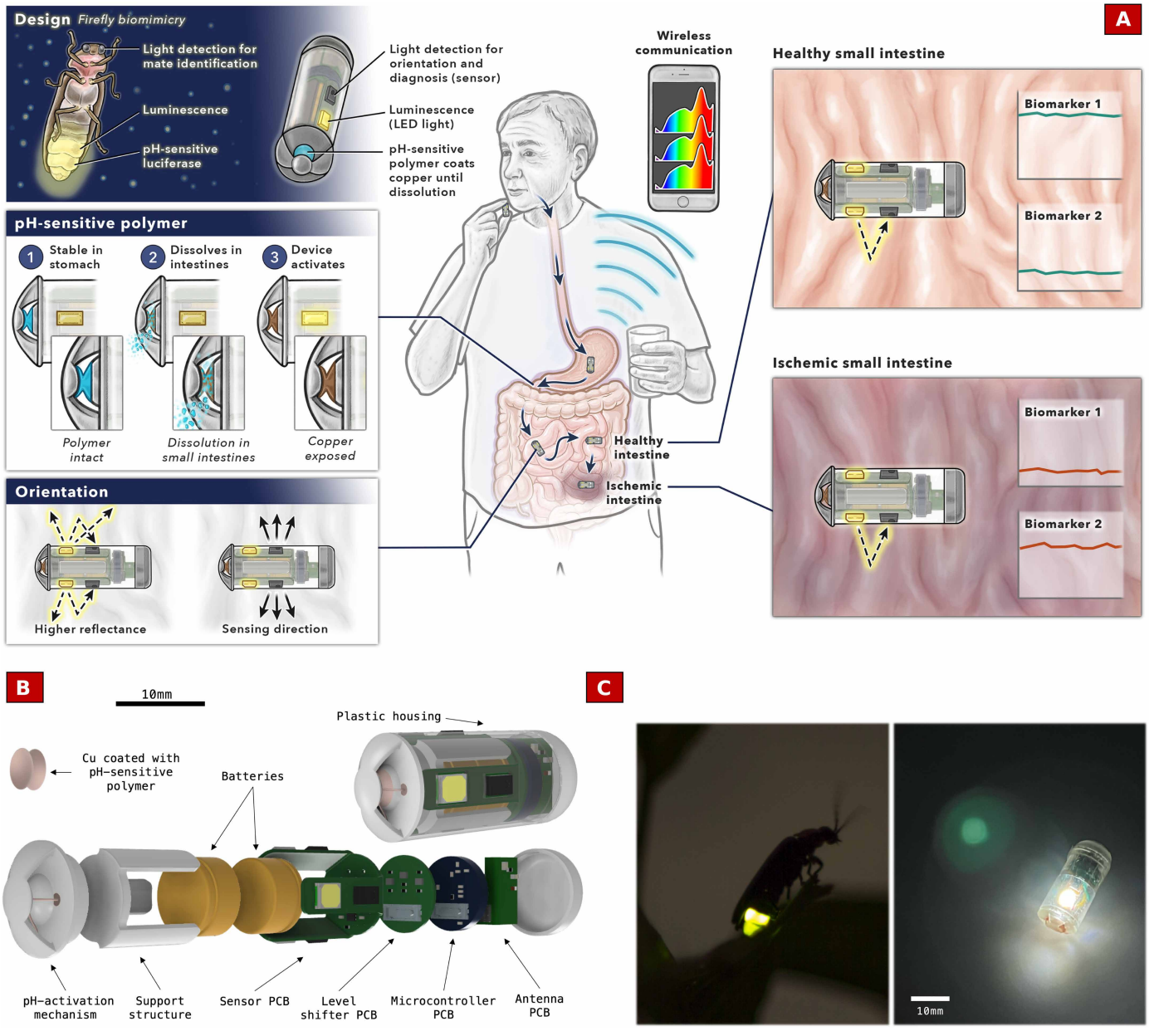

Fig. 1. Overview of the bioinspired design of the ingestible device for diagnosing mesenteric ischemia. (**A**) Illustration of device operation. (**B**) Exploded and assembled computer-aided design (CAD) models of device (26.2-mm length and 11.0-mm diameter). (**C**) Photographs of device and bioinspiration.

of 85% ($n = 9$). We explored color change as an alternative biomarker but found that color change is only consistent on the outside of ischemic SI, not the inside. For device safety, the device was tested in ambulatory swine, showing safe GI transit with no contraindications ($n = 3$). Last, for communication, we demonstrated consistent 2.4-GHz wireless transmission from inside the SIs of swine to an external mobile phone, enabling the device to send its diagnosis to a patient.

RESULTS

Mesenteric ischemia causes reduction in tissue luminance

To induce mesenteric ischemia in swine, the mesenteric blood vessels proximal to the device's location were clamped (Fig. 2, A to E). The experiments were performed first on a pilot cohort ($n = 3$) to determine the target biomarker and diagnostic threshold. The same threshold was used on the test cohort ($n = 6$) to validate the target biomarker. The test cohort used the ingestible device (Fig. 2B), whereas the pilot cohort used a slightly larger pilot device comprising the same LED and sensors to emit and detect light. In the pilot cohort (Fig. 2, F to J), multiple trials were conducted in the same animal at different sections of the SI.

For each of the 10 channels of sensor data, we applied the correction factors and offsets, then applied a transformation matrix to compute the biomarker (Fig. 2F). The correction accounts for mechanical components of the device that affect optical properties, whereas the transformation converts the 10 channels of data into a measure of illuminance onto the sensor. This method computes sensor illuminance in units of lux (how much light falls on the sensor surface), which is a measure of tissue luminance in units of candela per square meter (how much light is reflected by the tissue). The measurements of luminance are relative measurements, and the data are plotted in arbitrary units.

The onset of ischemia is rapid, usually within 5 to 10 min of clamping the SI. In the pilot cohort consisting of 24 trials in three swine, the luminance of ischemic SI decreased rapidly before stabilizing after 5 to 10 min (Fig. 2G). This is hypothesized to be caused by changes in absorption/reflection due to tissue damage and hemoglobin deoxygenation (further detailed in Discussion). After 20 and 40 min of clamping the SI, the difference between healthy and ischemic SIs was statistically significant ($^{***}P < 0.01$). From this, we selected the threshold for the luminance biomarker to maximize diagnostic accuracy in the pilot cohort, with values below the threshold indicating ischemia. The selected threshold was 85% of the average luminance of healthy tissue, resulting in a diagnostic accuracy of 89%, with a sensitivity of 98% and a specificity of 88% (fig. S2).

An aberration in the recorded data exists between 25 and 35 min for the ischemic dataset because of temporary failure of sensor communication in one animal; connection was lost to the sensor at ~25 min but was recovered by ~35 min, biasing the average luminance to the other trials during that period. The data loss occurred during the four trials of the first in vivo experiment. The pilot devices were connected to microcontrollers via an interintegrated circuit (I^2C) for data logging. During the period of 25 to 35 min, the microcontrollers dropped the connection to the sensors, and no data were logged. The missing data during this period were not imputed, resulting in the sudden decrease and increase. For subsequent in vivo experiments, we improved the mechanical and electrical connections between the pilot devices and the microcontrollers. No further data loss occurred in the subsequent experiments.

Another aberration was at time (t) = 0: Healthy and ischemic SIs should have comparable luminance before the onset of ischemia, yet ischemia tissue already showed lower luminance. This is because of the time delay after clamping; after clamping to SI, 1 to 3 min are required to position the jejunum and then reclamp or suture the abdominal incision. During this time, the jejunum is being positioned by researchers under surgical lighting, which adds random noise to the luminance measurements. Thus, although ischemia progresses during the first 1 to 3 min, measurements are not possible, resulting in the bias at $t = 0$.

Mesenteric ischemia causes inconsistent inner tissue color change

Qualitatively, the outside of an ischemic SI is visually striking, presenting as blue/purple/black in contrast with the pink/red of a healthy SI. Thus, color change has been suggested in the literature as a biomarker for mesenteric ischemia for ingestible devices (*21*). In the pilot cohort, we used the collected data at 10 wavelengths from 350 to 1000 nm to extrapolate a continuous color spectrum. From the color spectrum, we observed consistency in healthy SIs (Fig. 2H) but an increase in "blueness" in ischemic SIs (Fig. 2I). To measure this change, we tested biomarkers that sum the intensities of color at various wavelength bands. The 450- to 500-nm band showed initial promise (Fig. 2J), with statistically significant change after 20 min ($^{**}P = 0.008$) and 40 min ($^{**}P = 0.06$).

Unfortunately, statistical significance alone is insufficient; in the pilot cohort, the threshold that maximizes diagnostic accuracy only results in 65% accuracy, with a sensitivity of 37% and specificity of 93% (fig. S3). These results are further backed by qualitative observations that the color change was observed on the outside of an ischemic SI, but not on the inside (Fig. 2H, inset). This is hypothesized to be because the color change is caused by bruising that occurs primarily on the outer submucosa (further detailed in Discussion). In summary, color change is not a suitable biomarker of ischemia for ingestible devices, and we proceeded with the luminance biomarker for validation in the test cohort.

Device activates in the SI and communicates wirelessly

Here, we detail device characterizations to enable disease diagnosis during the entire SI transit and wireless communication. To achieve the necessary battery life, the device is duty cycled, with the LEDs off and the MCU in sleep mode while inactive. Although the SI transit time can range from 2 to 6 hours (*27*), the transit time for PillCam has a median of 4.6 hours (*28*), consistent with the transit time of 4.9 hours for solid meals in healthy male and female adults (*29*). With a duty cycle of 10%, the device has a battery life of 5.18 hours (Fig. 3, A and B), drawing 6 mA in sleep mode and 10 mA in active mode with one LED and sensor turned on. The device's coin-cell–sized Li-ion batteries maintain a sufficient operating voltage until 5.18 hours, at which point the voltage drops sharply and there is insufficient power to turn on the LEDs. Wireless communication is only required once to transmit the diagnosis, and this single instance has a negligible contribution to the power budget. Lower duty cycles may be used to further increase device battery life to support the diagnosis of ischemia that occurs distally in patients with low GI motility (Fig. 3C).

Recall that the proposed biomarker was identified in a pilot cohort with a larger pilot device. The proposed device was designed with a diameter of 11.0 mm and is not expected to maintain contact

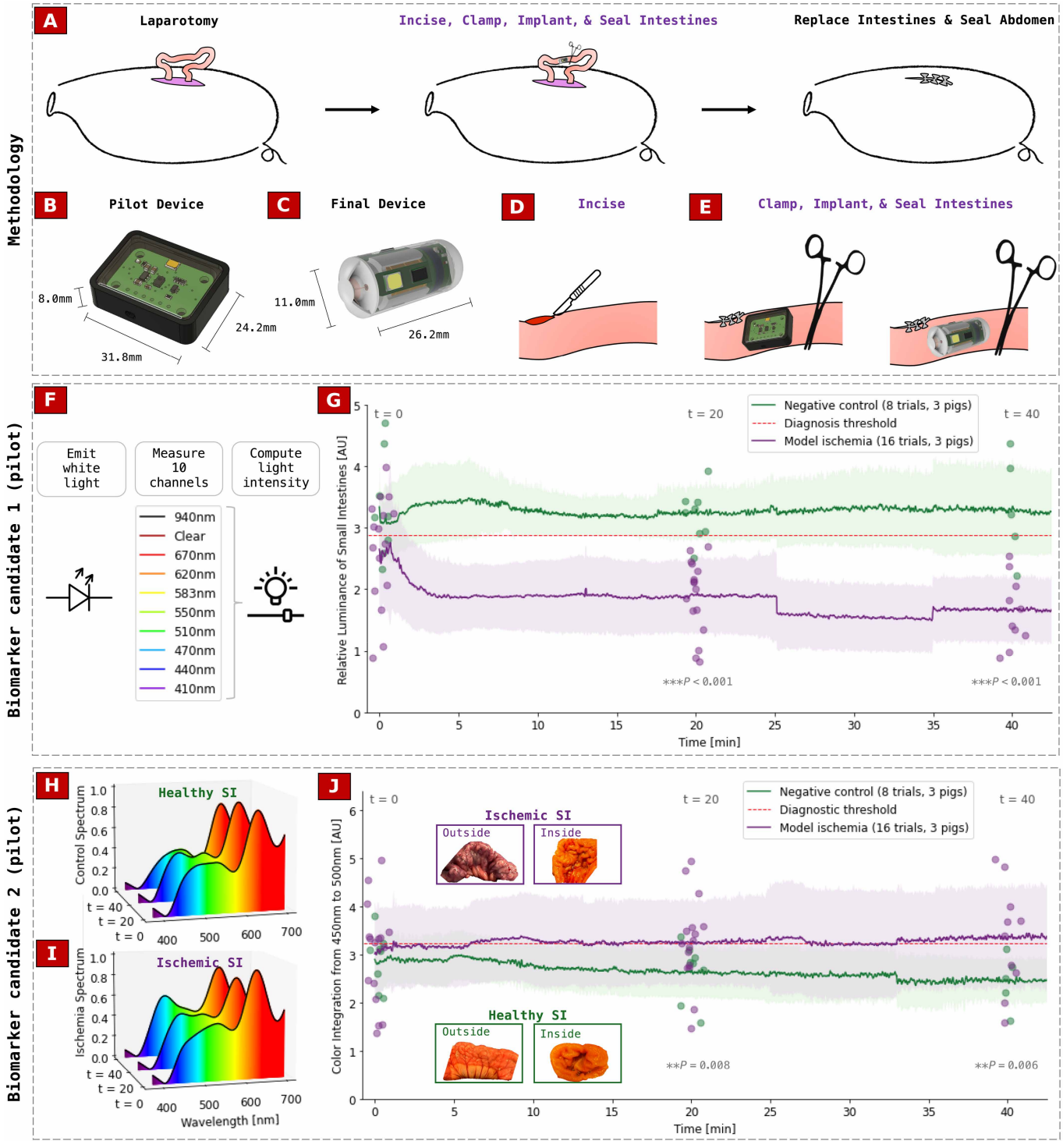

Fig. 2. In vivo swine study results with pilot device to determine biomarker for mesenteric ischemia. (**A**) Illustration of the in vivo swine experiment procedure to induce mesenteric ischemia. (**B**) CAD model of the noningestible pilot device used in the pilot cohort. (**C**) CAD model of the ingestible device used in the test cohort. (**D**) Illustrated procedure to implant the device. (**E**) Illustration of procedure to induce mesenteric ischemia by clamping blood vessels. (**F**) Illustration of sensing principle to compute the luminance biomarker. (**G**) Pilot cohort evaluation of luminance as a biomarker of mesenteric ischemia for 24 trials conducted in three pigs. (**H**) Sample pilot cohort color spectrum of healthy swine jejunum measured in vivo. (**I**) Sample pilot cohort color spectrum of ischemic swine jejunum measured in vivo for 24 trials conducted in three pigs. (**J**) Pilot cohort evaluation of color change as a biomarker of mesenteric ischemia. AU, arbitrary units.

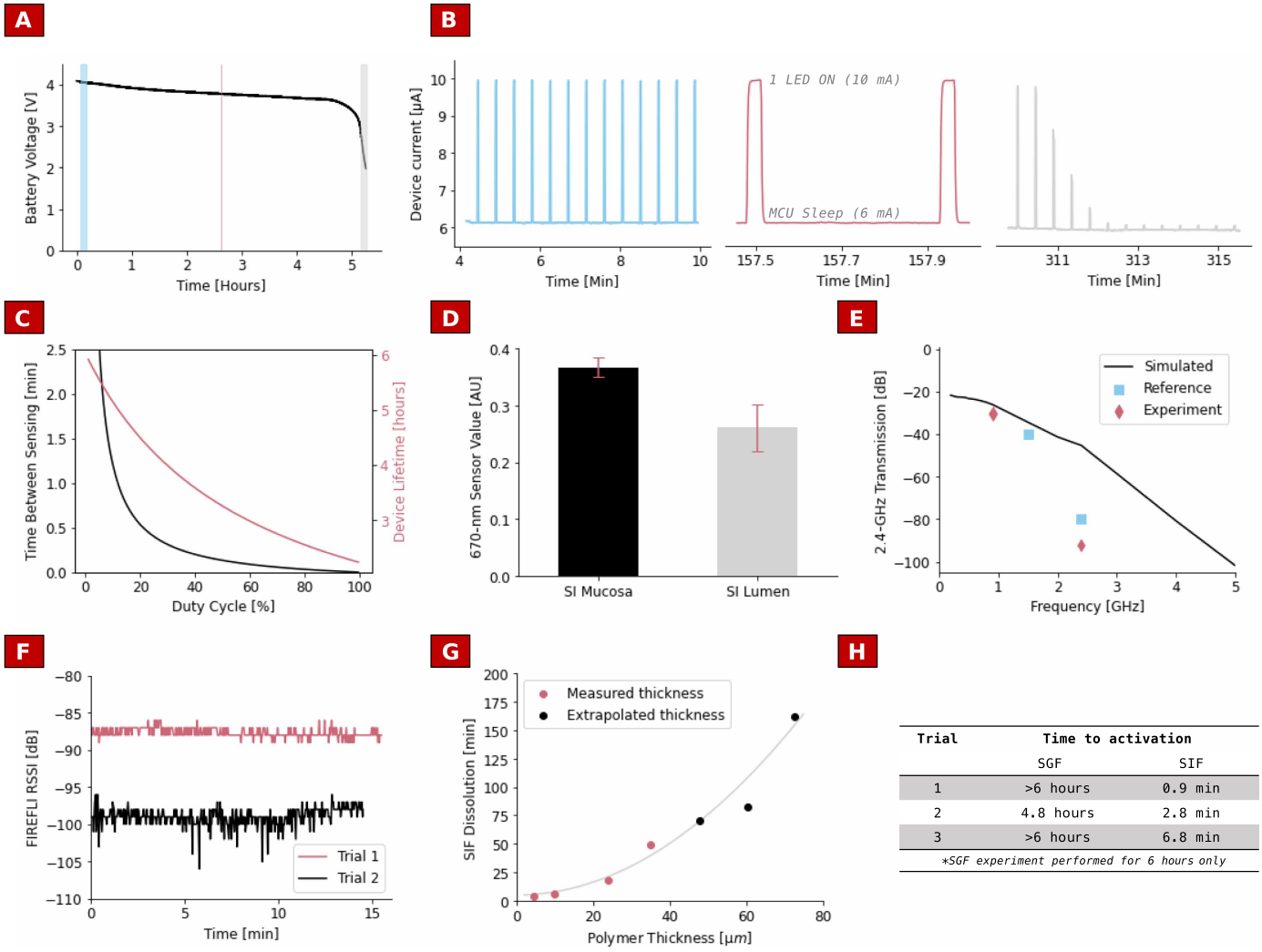

Trial	Time to activation	
	SGF	SIF
1	>6 hours	0.9 min
2	4.8 hours	2.8 min
3	>6 hours	6.8 min

*SGF experiment performed for 6 hours only

Fig. 3. Electrical and chemical characterizations informing device design. (**A**) Battery voltage during device operation with LEDs/sensors at a 10% duty cycle. Data for (A) and (B) were measured concurrently. (**B**) Device current during operation with LEDs/sensors at a 10% duty cycle. (**C**) Device lifetime with duty cycling. (**D**) Ex vivo evaluation of luminance as a method to determine contact with porcine SI mucosa. Results were collected from in vivo swine experiments, with error bars indicating the SD of 12 readings on the same tissue. (**E**) Wireless transmission loss from simulation, references, and in vivo swine experiments. References are plotted at 1.5 GHz (*51*) and 2.4 GHz (*53*). (**F**) Wireless data transmission strength of the ingestible device collected from in vivo swine experiments. The two trials were conducted in two different animals in a terminal setting. (**G**) Dissolution time of pH-sensitive polymer versus polymer thickness. (**H**) In vitro evaluation of device activation after dissolution of pH-sensitive polymer in SIF, turning on the electronics (SIF).

with SI mucosa in humans, which has an inner diameter averaging 25 mm (*30*), in the same way. The device was designed with three arms, each holding an LED/photodiode pair to emit and detect light, but the device must be capable of selecting the side with optimal contact. We found that the SI mucosa reflects more light than the SI lumen (Fig. 3D) in an ex vivo experiment with swine jejunum. Thus, to determine the side of optimal contact in the test cohort, the device is set to pulse and read from each of the three sides, selecting the side with the highest luminance for disease diagnosis.

For wireless communication, we studied the path loss of electromagnetic waves at frequencies commonly used in medical devices through simulation, in vivo experimentation, and comparison to literature (Fig. 3E). The simulation indicated an increase in transmission through the GI tract issue model at lower frequencies, consistent with the electrical permittivity and conductivity of human tissue known to vary with frequency. The simulated results did not account for potential losses due to efficiency, alignment, or impedance mismatches. Our measurement results for the 915-MHz and 2.4-GHz frequencies aligned with findings from previous studies, showing similar levels of transmission. At 2.4 GHz, the measured path loss was higher than the theoretical limit. This discrepancy is due to frequency shifts and changes in transmission characteristics when the chip antenna is placed near tissue. Further dynamic adjustments of the operating frequency and active impedance matching could enhance transmission at this frequency.

Despite this drawback, operating at 2.4 GHz offers an advantage for miniaturization, given that the shorter wavelength allows for a more compact antenna design (*31*) at a more common

communication protocol (*32*). For effective radiation, the electric current path should be approximately a quarter wavelength of the antenna's size, directly correlating with frequency. However, miniaturizing the antenna to fit within the constraints of an ingestible device compromises this relationship, leading to reduced radiation efficiency due to the inverse correlation between frequency and antenna size. To validate the feasibility of 2.4-GHz communication, a prototype device with the same MCU and antenna as the final device was implanted in swine jejunum during an in vivo experiment; the device demonstrated consistent wireless data transmission to an external mobile device for the duration of the 30-min experiment (Fig. 3F). Thus, 2.4 GHz was selected as the communication frequency.

To prevent unnecessary power consumption, the device must not activate before entering the SI. This has the additional benefit of preventing inappropriate diagnoses in the esophagus or stomach. To achieve this, we used the Eudragit L100-55 polymer, which is designed to degrade in the pH of the SI, but not in the pH of the esophagus and stomach. Eudragit L100-55 has similar dissolution profiles in both human and porcine pH ranges on the basis of prior reports (*33*–*35*). In vitro experiments showed that the time of dissolution in simulated intestinal fluid (SIF), with a pH of ~6.8, can be tuned via thickness (Fig. 3G). At a thickness of 30 μm or more, the polymer showed stability in simulated gastric fluid (SGF), with a pH of ~1.2, even after 6 hours of immersion. On the device, 30 μm of the polymer was spray coated between copper foil (thickness measured with a profilometer), which, upon dissolution, completes the electrical connection to the batteries. This activation mechanism was validated in vitro with prototype devices, which were placed in SGF or SIF; if the mechanism activates, then an LED is connected to the battery and turns on (fig. S4). The results of this experiment suggested stability in SGF after 6 hours and dissolution in SIF after 3.5 ± 3.0 min (Fig. 3H). The disparity in SGF activation time in trial 2 is likely because of inconsistencies in device assembly and fabrication that affect the exposure of the Eudragit-L100-55 to the SGF.

Device enables accurate and safe diagnosis

We validated the proposed biomarker, threshold, and device design in a test cohort of $n = 6$ swine with one healthy and one ischemia trial in each animal. The device can select the sensing direction by determining the side of best contact—that is, the side with the highest luminance—in both healthy (Fig. 4A) and ischemic (Fig. 4B) jejuna. Notably, one unselected side in the sample healthy data (Fig. 4A) is below the diagnostic threshold. Without the determination of contact, the device would have made a false-positive prediction in this trial. However, for most trials in the test cohort, the device maintained mucosal contact on all sides. Qualitatively, the device tended to fit snuggly inside the jejunum; in some cases, the swine jejunum was bloated, and the device would not have made mucosal contact on all sides, but the implantation procedure required an incision, deflating the jejunum.

In the test cohort, the device accurately diagnosed mesenteric ischemia using the threshold of luminance selected in the pilot cohort (Fig. 4C). As before, the onset of ischemia was rapid, usually within 5 to 10 min of clamping the SI. After 10 min of clamping the SI, the difference between healthy and ischemic SIs was statistically significant ($^{***}P < 0.01$). Across the entire test cohort, the device achieved a diagnostic accuracy of 91%, with a sensitivity of 98% and a specificity of 85% (fig. S5). From the pilot cohort, the sample size required for 80% statistical power (Cohen's *D*) was two for the luminance biomarker; thus, the test cohort had sufficient statistical power. Additionally, wireless transmission from the device was tested successfully in two animals of the test cohort, enabling communication to an external mobile phone or antenna receiver (table S6).

To validate the safety of the device, we performed in vivo survival experiments in $n = 3$ ambulatory swine. The device was delivered to the stomach via an overtube under anesthesia, and x-ray images were taken in the subsequent days. In all trials, the x-ray images showed device passage inside the GI tract (Fig. 4D and fig. S6), and the animals were monitored for adverse effects showing no contraindications (Fig. 4E). In two of the three trials, the device was recovered successfully after passage. In these two trials, inspection showed that the device retained its mechanical integrity with no biofouling or damage to the internal electronics (fig. S7), demonstrating safe passage.

DISCUSSION

AMI is associated with high morbidity and mortality, often because of diagnostic delays, given its nonspecific symptoms, and limitations of current diagnostic modalities, which are complex, costly, and invasive and frequently require specialized staff, equipment, and facilities. There is a critical need for alternative diagnostic approaches that are accurate, rapidly accessible, cost effective, and minimally invasive.

We proposed two potential biomarkers of mesenteric ischemia for ingestible devices: tissue luminance and color. Although the former enabled accurate diagnosis, the latter performed poorly and was prone to false-negative results. The device estimates luminance using 10 wavelengths of light across the visible spectrum. With fewer channels or a narrower spectrum, luminance cannot be accurately estimated, with higher percentage errors as channels of data are eliminated (fig. S8).

Tissue luminance measures how much the emitted light illuminates the tissue, with ischemic tissue demonstrating lower luminance. The reduction in luminance may be explained by a combination of factors. First, ischemia may lead to a disorganized, dense tissue structure because of the ischemic cascade, which causes mitochondrial damage, cell membrane damage, and a buildup of metabolic waste (*36*), resulting in tissue damage and hypoxia (*37*); consequently, ischemic tissue may reflect or scatter less light. In contrast, healthy tissue may exhibit an organized structure with intact cells (*38*), which may reflect or scatter more light and informs the technique of diffuse reflectance spectroscopy to differentiate the type of colon tissue (*39*). Second, ischemia involves a reduction in blood supply to tissues, resulting in reduced delivery of nutrients to tissues as well as localized hypoxia. Deoxygenated hemoglobin absorbs more red light and less infrared light than oxygenated hemoglobin (*40*), resulting in lower luminance from light near this wavelength. The experiments used white LEDs shining light across the visible spectrum, but the absorption of deoxygenated hemoglobin across the full visible spectrum was not well characterized. However, we explored color change in the red wavelengths and found it insufficient to reliably detect mesenteric ischemia, suggesting that deoxygenated hemoglobin may absorb more light than oxygenated hemoglobin at other wavelengths in the visible spectrum. To better understand the underlying mechanism behind the reduction in luminance in ischemic tissue, future work will correlate histology with ex vivo spectroscopy.

Color change has been proposed in literature as a diagnostic for mesenteric ischemia, with one patent suggesting using wavelengths

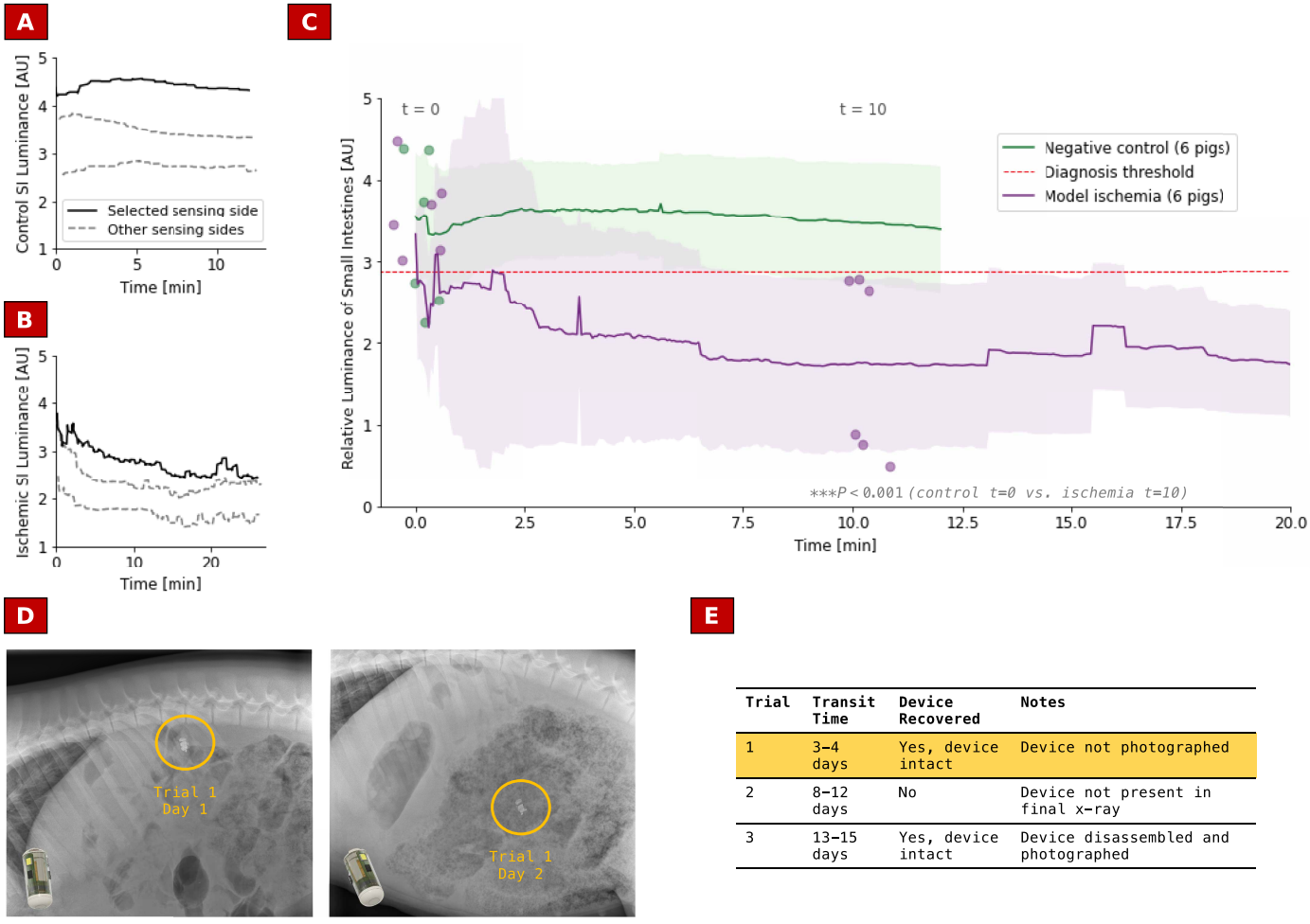

Trial	Transit Time	Device Recovered	Notes
1	3–4 days	Yes, device intact	Device not photographed
2	8–12 days	No	Device not present in final x-ray
3	13–15 days	Yes, device intact	Device disassembled and photographed

Fig. 4. In vivo swine study results with pilot device to validate biomarker for mesenteric ischemia. (**A**) Sample luminance biomarker values for healthy swine jejunum using a capsule with sensors on three sides. The black line is the side with best contact to the tissue. (**B**) Sample luminance biomarker values of ischemic swine jejunum using a capsule with sensors on three sides. The black line is the side with best contact to the tissue. (**C**) Test cohort validation of luminance as a biomarker of mesenteric ischemia for 12 trials conducted in six pigs. AU, arbitrary units. (**D**) Selection of x-ray images from the in vivo swine experiment verifying safe passage of the device. "Trial 1" in (D) and (E) refers to the same experiment. (**E**) Result of in vivo swine studies verifying safe passage of the device for three trials conducted in three pigs. "Transit time" refers to the minimum number of days postingestion after which the device is no longer present in the GI tract.

of 540 to 620 nm (*21*). However, experimental results show that color change was only observed on the serosal surface of intestinal tissue. On the interior/luminal surface, it often appeared similar in color to healthy tissue, making this an unsuitable biomarker for ingestible devices. This is hypothesized to be because color change is caused by bruising (*41*), which is caused by injury to the blood vessels surrounding tissue. The outer surface (serosa) of the SI contains larger blood vessels compared with the capillaries of the inner villi (*42*). Thus, the serosa would be expected to undergo bruising and color change, whereas the effect may be more limited on luminal/mucosal surfaces. However, additional experiments would be required to validate this hypothesis.

The main strength of this study is the validation in a large sample size with sufficient statistical power. The limitations of the study include the lack of validation in ambulating animals. Long-term monitoring in ambulating animals may provide additional diagnostic insights, especially in cases of borderline or progressive ischemia. The method for modeling mesenteric ischemia is severe and can only be performed in terminal settings under euthanasia.

For clinical translation, the proposed capsule (11.0 mm by 26.2 mm) is comparable to the PillCam SB3 (11.4 mm by 26.2 mm), a widely used, US Food and Drug Administration–approved ingestible capsule. Therefore, it is expected to be well tolerated. However, PillCam has a median gastric transit time of 58 min and SI transit time of 4.6 hours (*28*), resulting in a delayed diagnosis, especially if the site of ischemia is distal. However, this transit time can be greatly increased if the device is ingested with prokinetic agents (*43*). With a faster transit time, capsule orientation and movement may influence the quality of sensor acquisition. For orientation, the device can select the side of best contact using the 670-nm channel (Fig. 3C); side selection prevents diagnosis on a side with poor contact, which may lead to false-positive or false-negative results (Fig. 4, A and B). For movement, human SI transit speed is not well characterized, but we estimate that an average transit speed of 0.5 mm/s

would be typical based on SI length (*44*) and SI transit time (*45*). Using the ingestible device on phantom GI tissue, we show that device movement at <10 mm/s leads to an SD of <0.04 in sensor values of the 670-nm channel (fig. S9); for healthy tissue, a typical magnitude of the 670-nm channel is 0.3 (fig. S10), suggesting that the capsule introduces a low but nonnegligible error. This error may be compensated with higher sensor sampling rates at the cost of higher power consumption.

For safety and biocompatibility, the in vivo survival studies demonstrated safe passage with no adverse effects. The ingestible device was fabricated inside a 3D printed casing (BioMed clear resin, Formlabs) with an acrylic window for the sensors and sealed with a UV (ultraviolet)–cure epoxy (AA352, Loctite). Both the BioMed clear resin (*46*) and the acrylic window are biocompatible (*47*). AA352 epoxy is intended for industrial use, but similar UV-cure epoxies are biocompatible assuming sufficient curing (*48*).

MATERIALS AND METHODS

In vivo studies

Animal experiments were performed in accordance with protocols approved by the Committee on Animal Care at the Massachusetts Institute of Technology (IACUC protocol number 2207000395) and the Institutional Animal Care and Use Committee at Accuro Farms (IACUC protocol number AZ003). Experiments were performed in swine, because their GI anatomy is comparable to that of humans and because they are widely used as an in vivo model to evaluate medical devices in the GI tract. Experiments were performed with 10 Yorkshire swine (CBSET Inc., Grafton, MA) aged 5 to 9 months and weighing 60 to 100 kg. Nine swine were female, and one was male.

Experiments involving sensor measurements of healthy or ischemic SI were conducted in a terminal or nonsurvival setting under general anesthesia. Animals were fasted overnight. Pigs were sedated with Telazol (5 mg/kg, tiletamine/zolazepam) and xylazine (2 mg/kg), intubated, and maintained on 1 to 3% isoflurane in oxygen. Anesthetized animals were placed in dorsal recumbency on a heated surgical table for thermal support. Heart rate, respiratory rate, end-tidal CO_2, peripheral oxygen saturation (SpO_2), noninvasive blood pressure, and body temperature were monitored, and intravenous fluids were provided to maintain adequate hydration of the animal. Local subcutaneous infiltration with lidocaine or bupivacaine was performed before making a surgical incision for local anesthesia. The jejunum was accessed via midline laparotomy. An incision of ~1 cm was made in the jejunum, and the pilot or test device was inserted ~10 cm into the jejunum. The incision was then sealed via suture or via clamping. In ischemia trials, two hemostatic clamps were placed across the mesenteric vessels supplying the section of jejunum of interest. In all trials, the jejunum was then replaced into the abdomen along with any clamps, and the abdomen was sealed with additional clamps; these steps required 1 to 3 min and were performed under surgical lights in the operating room. The rapid repositioning of the jejunum and the background lighting added random noise to luminance measurements, so measurements were not recorded during this time. A surgical towel was placed over the swine's abdomen to maintain its body temperature, and the time at which this final step was completed is shown as $t = 0$ in all presented results.

Experiments involving device safety and GI transit were conducted in a survival setting. Pigs were fasted as described earlier and sedated with dexmedetomidine (0.03 mg/kg) and midazolam (0.25 mg/kg), intubated, and maintained on 1 to 3% isoflurane in oxygen. The device was delivered under anesthesia to the stomach endoscopically. The animal recovered, and radiographic images were acquired in the following days with the animal under sedation. Device retrieval after GI transit was attempted by radiographically examining all bedding material in the animal's enclosure.

Biomarker extraction

We analyzed two biomarkers for mesenteric ischemia: luminance and color change. Light reflectance data were gathered using AS7341 sensors (AMS), which contain photodiodes that measure light intensity across 10 spectral bands. At each sampling point, digital values were measured corresponding to the intensity of light at each wavelength. Correction factors and offsets provided by the manufacturer were applied to the raw sensor data as follows, which account for factors such as optical interference and spectral sensitivity differences between channels

$$\text{Sensor\_values} = [V1, V2, \ldots, V10]^T$$
$$\text{Correction\_offset} = [O1, O2, \ldots, O10]^T$$
$$\text{Correction\_factor} = [F1, F2, \ldots, F10]^T$$
$$\text{Corrected\_values} = \text{Correction\_factor} \times (\text{Sensor\_values} - \text{Correction\_offset})$$

where T is the vector transpose operator. To avoid confusion, we clarify here that we calculated the illuminance on the sensor in units of lux (how much light falls on the sensor surface); this calculation of illuminance is a measure of tissue luminance in units of candela per square meter (how much light is reflected by the tissue). Illuminance is what is computed, whereas luminance is the actual biomarker. To calculate the illuminance in units of lux from a set of corrected sensor values, the data must first be transformed into the 1931 CIE (International Commission on Illumination) *XYZ* color space using a calibration matrix. Within the *XYZ* color space, the *Y* component represents luminance, and lux is determined by multiplying the ratio of the *Y* component to the sum of all components by 683

$$[X, Y, Z] = XYZ\_\text{Calibration\_Matrix} \times \text{Corrected\_Values}$$
$$\text{Illuminance\_Lux} = (Y/[X + Y + Z]) \times 683$$

The color biomarker was calculated through the multiplication of corrected sensor values with a 720 -by-10 spectral calibration matrix, where each row of the matrix represents a 1-nm increment across the color spectrum. The resulting values were normalized to the maximum spectral value. The color data were then derived by summing the spectral values corresponding to the desired wavelength range; 450 to 500 nm was selected because it represented a change in the blueness of ischemic tissue

$$\text{Spectrum} = \text{Spectral\_Calibration\_Matrix} \times \text{Corrected\_values}$$
$$\text{Normalized\_spectrum} = \text{Spectrum}/\text{MAX}(\text{Spectrum})$$
$$\text{Color} = \text{Sum of Normalized\_specturm}$$

To calculate the effect of the number of sensor channels on biomarker estimation accuracy, we used the following method. The raw data were multiplied into a spectral calibration matrix provided by the manufacturer (AMS) to construct a normalized color spectrum [S(λ)] with a 1-nm step size from 410 to 750 nm. Each value in the spectrum was multiplied by CIE color matching functions [X(λ), Y(λ), and Z(λ)] (*49*) and LED lamp illuminant tables [I(λ)] (*50*) and then integrated across the wavelength range to transform the reconstructed spectrum to the CIE 1913 *XYZ* color space. The *XYZ*

coordinates were normalized, and the *Y* coordinate was multiplied by 683 to yield the final value in units of lux

$$X = \int X(\lambda)\cdot I(\lambda)\cdot S(\lambda)\ d\lambda$$
$$Y = \int Y(\lambda)\cdot I(\lambda)\cdot S(\lambda)\ d\lambda$$
$$Z = \int Z(\lambda)\cdot I(\lambda)\cdot S(\lambda)\ d\lambda$$
$$\text{Lux} = (Y/[X + Y + Z]) \times 683$$

To simulate a device with fewer sensor channels, this process was modified to compare the sensor channels of the device against a lesser number of channels (fig. S8). The same raw sensor data were multiplied directly into the CIE color matching and reference illuminant functions and then integrated across the sensor's wavelength range to compute luminance. This process was repeated, whereby, for each repetition, one channel was omitted from the *XYZ* and lux computation.

To verify sensor calibration, we performed baseline measurement with reference colors. A test device with an LED set to 4 mA and a photodiode sampling at 25 Hz was used. The device was used to make measurements of seven different colors of construction paper (993200, Crayola). Sensor output values were then converted into a color spectrum as previously described. The results showed a distinct shift in the spectrum corresponding to color (fig. S11).

To verify sensor detection of motion, a test capsule was attached to a robotic arm (Braccio, Tinkerkit) and moved across synthetic gastric tissue (141670, SynDaver). A test device with an LED set to 4 mA and a photodiode sampling at 25 Hz were used. Data were recorded for a stationary trial and nine moving trials with varying device speed, starting from the estimated SI transit speed [0.5 mm/s based on SI length (*44*) and SI transit time (*45*)]. The SD of the 630-nm channel was plotted against device speed (fig. S9).

Electrical design and characterization

The device contains four PCBs for the antenna, MCU, level shifter, and LEDs/sensors. The PCBs were manufactured and assembled by Rush PCB (Milpitas, CA) and stacked axially using mezzanine connectors. The boards were powered by two coin-cell–sized Li-ion batteries (LPM0840, LiPol) connected in parallel. The antenna and MCU boards together contained an nRF5340 system-on-chip MCU (Nordic Semiconductor) and a 2.4-GHz chip antenna (2450AT07A0100, Johanson Technology). The MCU board was rigid with six layers, whereas the antenna board was flexible, enabling the chip antenna to bend and an air gap around the chip antenna.

To determine the device's power profile and to verify the device's battery life, the final electronics were used with LEDs/sensors operating at a 10% duty cycle. The MCU, sensor, and level-shifting PCBs were powered by two LPM0840 LiPo batteries charged to 4.2 V and connected in parallel. Current consumption was monitored using an ammeter (Power Profiler Kit II, Nordic Semiconductor), and battery voltage during discharge was recorded with a voltmeter (34470A Digital Multimeter, Keysight).

Although the nRF5340 is capable of voltage regulation, we observed inconsistent behavior in low-power mode. When designing the PCB containing the MCU, we made the decision to omit some components required for operating the switching converters. This was a trade-off between size and power consumption. However, we believed that not using the switching converter caused issues when trying to configure the chip to operate at different input/output (I/O) voltages. Thus, the next board was a level shifter that intercepted the 3.3-V I^2C signal output from the MCU, shifting the logic level down to 1.8 V. The final board contained three arms, each with a white LED and an AS7341 sensor that bent at a 90° angle. The main body of the sensor board contained vias for the 3.3-V input and ground pins, which were used for connections to the batteries and the pH-activation mechanism. Raw sensor values from the sensors were passed through the level-shifting board, recorded by the MCU, and transmitted to an external device via the antenna. Power profiling was performed using the Power Profiler Kit II (Nordic Semiconductor).

Firmware was built using the nRF Connect SDK in Visual Studio Code. The signals from 10 channels were routed to a six-channel analog-to-digital converter via a super multiplexer configured by the device firmware. The LEDs were set to 4-mA power consumption. The MCU switched between sleep and active mode, and it performed sensor control and biomarker extraction (fig. S1). Initial firmware for wireless communication used the Nordic UART Service (NUS), which emulates a serial port over Bluetooth. Although this worked during in vivo swine animal experiments, NUS requires a constant connection between the device and the external mobile device, meaning communication would stop even if the connection was only briefly lost. A constant connection was not required, because the device only needed to transmit its diagnosis and did not need to receive any data. Thus, the final firmware for wireless communication used the Bluetooth Mesh networking standard, allowing the device to advertise messages to be read by an external receiver.

Wireless communication experiments

To evaluate the feasibility of wireless transmission at different frequencies, we performed simulations and in vivo experiments. Simulations were performed in CST Studio Suite (Dassault Systems). The simulation component used a detailed four-layer GI tract tissue model, which included the skin, fat, muscle, and stomach layers, set up in a method similar to that in previous work (*51*) with dielectric properties from an established database (*52*). This model was used to evaluate wave transmission across a broad frequency range from 200 MHz to 4 GHz. We introduced a plane wave with normal incidence via waveguide ports at the stomach layer and measured the transmission from the skin layer. To enhance the realism of the model, appropriate air gaps were included, which helped simulate the actual conditions in the human body.

In vivo experiments were performed in swine with protocols approved by the Committee on Animal Care at the Massachusetts Institute of Technology. We investigated key industrial, scientific, and medical bands: 902.8 to 928 MHz and 2.4 to 2.5 GHz. The transmitter millimeter-sized antennas (2450AT07A0100, Johanson Technology for 2.4 GHz, M620720, Kyocera AVX for 915 MHz) were designed for far-field operation and positioned in the stomach after laparotomy. The receiver used two different panel antennas for 915 MHz and 2.4 GHz that were placed roughly 10 cm away from the animal.

For testing wireless communication with the device, we tested communication to both an external mobile phone (iPhone 13) and a receiver antenna (MD24-12 panel antenna, TE Connectivity with SH24Gi4000 signal booster, Sunhans) connected to an nRF5340 development kit. Connection to the mobile phone was established using the nRF Connect mobile application. A message containing sensor data was transmitted, and the received signal strength indicator from each message was recorded. In all experiments, the receiver device was placed on top of a blanket, which, in turn, was placed on top of the swine's abdomen.

pH-activation mechanism

For the initial in vitro test, glass slides were spray coated (Exacta-Coat, Sono-Tek) with a solution of 5 g of Eudragit L100-55 dissolved

in 40 ml of isopropanol and 60 ml of acetone. The thicknesses of coatings of less than 40 μm thick were measured using a profilometer (VK-X3050, KEYENCE). The thicknesses of coatings of greater than 40 μm thick were extrapolated using the number of spray-coater passes (fig. S12) with a linear fit [coefficient of determination (R^2) = 0.997]. The solvents were allowed to evaporate after spray coating. For the device, copper foil with conductive adhesive was spray coated with the same polymer. Dissolution testing was performed with SGF (7108-16, Ricca) and SIF (7109.75-16, Ricca). Time-lapse videos captured the timing of the dissolution or lack thereof. Device assembly was performed by hand, and coatings may have been inadvertently scratched, leading to variation in dissolution times in SGF and SIF.

The capsule cap for the device held the dissolution mechanism. It was 3D printed (Objet 260 Connex 3, Stratasys) to hold the polymer-coated copper. The cap held two hemispherical foil mounts whose peaks were spaced 350 μm apart. One hemisphere protruded from the base of the cap, whereas the other was suspended above it by thin, deformable walls. When the gap between the hemispheres was increased, the walls applied a small spring force to the upper hemisphere, pushing it to its initial position. Two stacked pieces of polymer-coated copper foil had a thickness of 600 μm. When the pieces were placed between the hemispheres, a constant pressure was exerted on the tape, ensuring adequate contact. Upon dissolution, the copper pads completed the circuit, turning on the electronics (fig. S4).

Device fabrication and assembly

The pilot device used was an AS7341 Breakout Board (Adafruit) with the Qwiic connectors removed. The device was protected by a 3D printed case (BioMed clear resin printed with Form 3, Formlabs) and covered by a clear, acrylic panel. UV-cure epoxy (AA352, Loctite) was applied to limit moisture ingress. Wires measuring ~1.5 m extended from the pilot device for powering and serial communication. This device measured 31.8 mm by 24.2 mm by 8.0 mm and was inserted surgically for data collection.

The test device had a 3D printed outer body (Form 3, Formlabs) with cutouts for the white LEDs and AS7341 sensor with multichannel photodiodes. The capsule cap with the dissolution mechanism was 3D printed (Stratasys). The device was assembled by first stacking two 3.8-V Li-ion batteries (LPM0840, LiPol Battery) soldered in parallel. The PCBs for the antenna, microcontroller, level shifter, and sensor board were assembled via mezzanine connectors to form one stack, with the sensor board at the bottom. The batteries were placed below the sensor PCB, and the arms of the sensor PCB were folded upward at a 90° angle. The negative terminal of the battery was soldered to a pin on the sensor board. The positive terminal of the batteries and a wire from a pin on the sensor board protruded from this assembly. The stack of PCBs and batteries was placed into the 3D printed outer body.

The capsule cap held the device activation mechanism. Two 3-mm–by–3-mm pieces of polymer-coated copper foil were cut. The protruding wires were attached to the back of the copper foil via adhesives. The foil pieces were then inserted into the gap on the cap and secured with adhesives, oriented to ensure that the polymer-coated sides of the copper foil made contact. All components and holes for the protruding wire were sealed using UV-cure epoxy (AA352, Loctite), completing the assembly.

Data processing and statistical analysis

In the pilot cohort, there were 16 ischemia trials and 8 baseline trials. To evaluate the data in a balanced dataset, we randomly selected 8 of the 16 ischemia trials. In both the pilot and test cohorts, baseline trials were recorded for less time than ischemia trials. For baseline trials, we randomly sampled 50 data points in each trial. For ischemia trials, we randomly sampled 50 data points after 10 min in each trial because we considered ischemia to have been fully induced after 10 min. Statistical significance between the healthy and ischemia groups was determined via Student's *t* test.

In the pilot cohort, we selected optimal diagnostic thresholds for the luminance and color biomarkers. These thresholds were identified by sweeping the range from the minimum to maximum biomarker values and then identifying the value with the highest classification accuracy. Data from all trials were tested against these thresholds to compute true-positive, false-negative, true-negative, and false-positive results for each biomarker. In the pilot cohort, combinations of the luminance and color-change biomarkers were tested, but no combination resulted in a higher diagnostic accuracy than using the luminance biomarker alone. *P* testing was performed for each biomarker at $t = 0$, 20, and 40 min to evaluate statistical significance between ischemia trials versus healthy trials. Diagnostic accuracy, sensitivity, and specificity are reported for the individual cohorts as well as the combined cohort of $n = 9$; for the latter, the reported values were weighed by the population size of the cohorts.

In the test cohort, the device was preset to have the same sensor sensitivity as the pilot device. Validation of the test cohort used the same threshold as the pilot cohort. The biomarker's diagnostic threshold was not informed by data collected in the test cohort.

Supplementary Materials

This PDF file includes:

Figs. S1 to S12
Table S1

REFERENCES AND NOTES

1. K. Tamme, A. R. Blaser, K. T. Laisaar, M. Mändul, J. Kals, A. Forbes, O. Kiss, S. Acosta, M. Bjørck, J. Starkopf, Incidence and outcomes of acute mesenteric ischaemia: A systematic review and meta-analysis. *BMJ Open* **12**, e062846 (2022).
2. M. Bala, J. Kashuk, E. E. Moore, Y. Kluger, W. Biffl, C. A. Gomes, O. Ben-Ishay, C. Rubinstein, Z. J. Balogh, I. Civil, F. Coccolini, A. Leppaniemi, A. Peitzman, L. Ansaloni, M. Sugrue, M. Sartelli, S. D. Saverio, G. P. Fraga, F. Catena, Acute mesenteric ischemia: Guidelines of the World Society of emergency surgery. *World J. Emerg. Surg.* **12**, 38 (2017).
3. Mayo Clinic, "Intestinal ischemia - Symptoms and causes"; www.mayoclinic.org/diseases-conditions/intestinal-ischemia/symptoms-causes/syc-20373946.
4. Mayo Clinic, "Food poisoning - Symptoms and causes"; www.mayoclinic.org/diseases-conditions/food-poisoning/symptoms-causes/syc-20356230.
5. A. Amini, S. Nagalli, "Bowel ischemia," in *StatPearls [Internet]* (StatPearls Publishing, 2025).
6. H. Yu, I. D. C. Kirkpatrick, An update on acute mesenteric ischemia. *Can. Assoc. Radiol. J.* **74**, 160–171 (2022).
7. K. Peoc'h, A. Nuzzo, K. Guedj, C. Paugam, O. Corcos, Diagnosis biomarkers in acute intestinal ischemic injury: So close, yet so far. *Clin. Chem. Lab. Med.* **56**, 373–385 (2018).
8. M. Montagnana, E. Danese, G. Lippi, Biochemical markers of acute intestinal ischemia: Possibilities and limitations. *Ann. Transl. Med.* **6**, 341 (2018).
9. N. Treskes, A. M. Persoon, A. R. H. van Zanten, Diagnostic accuracy of novel serological biomarkers to detect acute mesenteric ischemia: A systematic review and meta-analysis. *Intern. Emerg. Med.* **12**, 821–836 (2017).
10. Z. Wang, J.-Q. Chen, J. Liu, L. Tian, A novel scoring system for diagnosing acute mesenteric ischemia in the emergency ward. *World J. Surg.* **41**, 1966–1974 (2017).
11. J. C. McRae, P. Jastrzebska-Perfect, G. Traverso, Challenges and opportunities for ingestible electronics across timescales. *Device* **1**, 100055 (2023).

12. C. Liatsos, S. Goulas, S. Karagiannis, E. Patelaros, D. Sabaziotis, C. Mavrogiannis, Diagnosis of small-bowel ischemic necrosis by capsule endoscopy. *Gastrointest. Endosc.* **62**, 439–440 (2005).
13. Z. Fireman, A. Glukhovsky, H. Jacob, A. Lavy, S. Lewkowicz, E. Scapa, Wireless capsule endoscopy. *Isr. Med. Assoc. J.* **4**, 717–719 (2002).
14. W. G. Kwack, Y. J. Lim, Current status and research into overcoming limitations of capsule endoscopy. *Clin. Endosc.* **49**, 8–15 (2016).
15. J. M. Stine, K. L. Ruland, L. A. Beardslee, J. A. Levy, H. Abianeh, S. Botasini, P. J. Pasricha, R. Ghodssi, Miniaturized capsule system toward real-time electrochemical detection of H_2S in the gastrointestinal tract. *Adv. Healthc. Mater.* **13**, e2302897 (2024).
16. H.-W. Huang, C. Ehmke, C. Steiger, I. Ballinger, M. Jimenez, N. Phan, H. Sun, K. Ishida, J. Kuosmanen, J. Jenkins, J. Korzenik, A. Hayward, G. Traverso, "In situ detection of gastrointestinal inflammatory biomarkers using electrochemical gas sensors," in *IEEE International Engineering in Medicine and Biology Conference* (*EMBC*) (IEEE, 2022), pp. 2491–2494.
17. K. Kalantar-Zadeh, K. J. Berean, N. Ha, A. F. Chrimes, K. Xu, D. Grando, J. Z. Ou, N. Pillai, J. L. Campbell, R. Brkljača, K. M. Taylor, R. E. Burgell, C. K. Yao, S. A. Ward, C. S. McSweeney, J. G. Muir, P. R. Gibson, A human pilot trial of ingestible electronic capsules capable of sensing different gases in the gut. *Nat. Electron.* **1**, 79–87 (2018).
18. Industrial Scientific, "Electrochemical gas sensor cross interference table"; www.indsci.com/en/blog/electrochemical-sensor-cross-interference-table.
19. K. F. Schuster, C. C. Thompson, M. Ryou, Preclinical study of a novel ingestible bleeding sensor for upper gastrointestinal bleeding. *Clin. Endosc.* **57**, 73–81 (2024).
20. K. Kato, Y. Iwasaki, M. Taniguchi, K. Onodera, M. Matsuda, S. Tamakawa, H. Furukawa, Nonocclusive mesenteric ischemia: Fulminant pancolitis. *Clin. Case Rep.* **4**, 307–309 (2016).
21. M. A. Imran, Optical capsule and spectroscopic method for treating or diagnosing the intestinal tract, US Patent 8,360,976 B2 (2013).
22. Medtronic, "PillCam SB 3 capsule endoscopy system"; www.medtronic.com/en-us/healthcare-professionals/products/digestive-gastrointestinal/capsule-endoscopy/endoscopy-systems/pillcam-sb-3-capsule-endoscopy-system.html.
23. M. M. Swindle, Ed., *Swine in the Laboratory: Surgery*, *Anesthesia*, *Imaging*, *and Experimental Techniques* (CRC Press, ed. 2, 2007).
24. I. S. Juel, E. Solligård, O. Lyng, T. Strømholm, K. E. Tvedt, H. Johnsen, P. Jynge, O. D. Sæther, P. Aadahl, J. E. Grønbech, Intestinal injury after thoracic aortic cross-clamping in the pig. *J. Surg. Res.* **117**, 283–295 (2004).
25. T. Yandza, M. Tauc, M.-C. Saint-Paul, M. Ouaissi, J. Gugenheim, X. Hébuterne, The pig as a preclinical model for intestinal ischemia-reperfusion and transplantation studies. *J. Surg. Res.* **178**, 807–819 (2012).
26. O. F. Bathe, A. W. C. Chow, P. T. Phang, Splanchnic origin of cytokines in a porcine model of mesenteric ischemia-reperfusion. *Surgery* **123**, 79–88 (1998).
27. Y. Y. Lee, A. Erdogan, S. S. C. Rao, How to assess regional and whole gut transit time with wireless motility capsule. *J. Neurogastroenterol. Motil.* **20**, 265–270 (2014).
28. J. Worsøe, L. Fynne, T. Gregersen, V. Schlageter, L. A. Christensen, J. F. Dahlerup, N. J. Rijkhoff, S. Laurberg, K. Krogh, Gastric transit and small intestinal transit time and motility assessed by a magnet tracking system. *BMC Gastroenterol.* **11**, 145 (2011).
29. R. Bennink, M. Peeters, V. Van Den Maegdenbergh, B. Geypens, P. Rutgeerts, M. De Roo, L. Mortelmans, Evaluation of small-bowel transit for solid and liquid test meal in healthy men and women. *Eur. J. Nucl. Med. Mol. Imaging* **26**, 1560–1566 (1999).
30. H. F. Helander, L. Fändriks, Surface area of the digestive tract - Revisited. *Scand. J. Gastroenterol.* **49**, 681–689 (2014).
31. R. E. Collin, F. J. Zucker, *Antenna Theory Part 2* (McGraw-Hill, ed. 1, 1968).
32. R. Ghanim, A. Kaushik, J. Park, A. Abramson, Communication protocols integrating wearables, ingestibles, and implantables for closed-loop therapies. *Device* **1**, 100092 (2023).
33. D. S. Miller, A. M. Parsons, J. Bresland, P. Herde, D. M. Pham, A. Tan, H. Hsu, C. A. Prestidge, T. Kuchel, R. Begg, S. M. Aziz, R. N. Butler, A simple and inexpensive enteric-coated capsule for delivery of acid-labile macromolecules to the small intestine. *J. Zhejiang Univ. Sci. B* **16**, 586–592 (2015).
34. C. Yu, H. Xu, X. Zhao, Q. Litke, J. Gong, C. Yang, S. Liu, Developing sodium metabisulfite (SMBS)-containing Eudragit L100-55 microparticles for controlled intestinal release of SMBS to detoxify deoxynivalenol. *Food Biosci.* **54**, 102859 (2023).
35. S. K. Jain, A. K. Jain, K. Rajpoot, Expedition of Eudragit polymers in the development of novel drug delivery systems. *Curr. Drug Deliv.* **17**, 448–469 (2020).
36. J. F. McNeer, J. R. Margolis, K. L. Lee, J. A. Kisslo, R. H. Peter, Y. Kong, V. S. Behar, A. G. Wallace, C. B. McCants, R. A. Rosati, The role of the exercise test in the evaluation of patients for ischemic heart disease. *Circulation* **57**, 64–70 (1978).
37. H. K. Eltzschig, T. Eckle, Ischemia and reperfusion—From mechanism to translation. *Nat. Med.* **17**, 1391–1401 (2011).
38. ScienceDirect, "Healthy tissue"; www.sciencedirect.com/topics/engineering/healthy-tissue.
39. S. N. Bess, G. J. Greening, T. J. Muldoon, Efficacy and clinical monitoring strategies for immune checkpoint inhibitors and targeted cytokine immunotherapy for locally advanced and metastatic colorectal cancer. *Cytokine Growth Factor Rev.* **49**, 1–9 (2019).
40. E. D. Chan, M. M. Chan, M. M. Chan, Pulse oximetry: Understanding its basic principles facilitates appreciation of its limitations. *Respir. Med.* **107**, 789–799 (2013).
41. Cleveland Clinic, "Bruises (ecchymosis)"; https://my.clevelandclinic.org/health/diseases/15235-bruises.
42. E. M. Fish, K. R. Shumway, B. Burns, "Physiology, small bowel," in *StatPearls [Internet]* (StatPearls Publishing, 2024).
43. Cleveland Clinic, "Prokinetic agents"; https://my.clevelandclinic.org/health/articles/prokinetic-agents.
44. M. Bekheit, M. Y. Ibrahim, W. Tobar, I. Galal, A. S. Elward, Correlation between the total small bowel length and anthropometric measures in living humans: Cross-sectional study. *Obes. Surg.* **30**, 681–686 (2020).
45. J. O'Grady, C. L. Murphy, L. Barry, F. Shanahan, M. Buckley, Defining gastrointestinal transit time using video capsule endoscopy: A study of healthy subjects. *Endosc. Int. Open.* **8**, E396–E400 (2020).
46. Formlabs, "BioMed clear resin"; https://formlabs.com/store/materials/biomed-clear-resin/.
47. S. M. Pituru, M. Greabu, A. Totan, M. Imre, M. Pantea, T. Spinu, A. M. C. Tancu, N. O. Popoviciu, I.-I. Stanescu, E. Ionescu, A review on the biocompatibility of PMMA-based dental materials for interim prosthetic restorations with a glimpse into their modern manufacturing techniques. *Materials* **13**, 2894 (2020).
48. Chase Corporation, "Resin designs"; https://chasecorp.com/resindesigns/uv-curable-adhesives/medical-device-adhesives/.
49. CIE, "CIE 1931 colour-matching functions, 2 degree observer" (International Commission on Illumination, 2019); https://doi.org/10.25039/CIE.DS.xvudnb9b.
50. CIE, "Relative spectral power distributions of illuminants representing typical LED lamps" (International Commission on Illumination, 2018); https://doi.org/10.25039/CIE.DS.vgssnyfg.
51. A. Abid, J. M. O'Brien, T. Bensel, C. Cleveland, L. Booth, B. R. Smith, R. Langer, G. Traverso, Wireless power transfer to millimeter-sized gastrointestinal electronics validated in a swine model. *Sci. Rep.* **7**, 46745 (2017).
52. IT'IS Foundation, "Dielectric properties"; https://itis.swiss/virtual-population/tissue-properties/database/dielectric-properties/.
53. Y. Jeon, S. Maji, S.-Y. Yang, M. S. S. Thaniana, A. Gierlach, I. Ballinger, G. Selsing, I. Moon, J. Jenkins, A. Pettinari, N. Fabian, A. M. Hayward, G. Traverso, A. P. Chandrakasan, "Secure and stable wireless communication for an ingestible device," in *2023 45th Annual International Conference of the IEEE Engineering in Medicine & Biology Society* (*EMBC*) (IEEE, 2023), pp. 1–6.

Acknowledgments: We thank V. E. Fulford, Alar Illustration, for Fig. 1A. **Funding:** This work was funded, in part, by (i) the Karl van Tassel (1925) Career Development Professorship, Department of Mechanical Engineering, Massachusetts Institute of Technology (MIT); (ii) the Division of Gastroenterology, Brigham and Women's Hospital; (iii) Advanced Research Projects Agency for Health (ARPA-H) under award number D24AC00040-00; and (iv) Defense Advanced Research Projects Agency (DARPA) under agreement number FA8650-21-2-7120 awarded to G.T. The views and conclusions contained herein are those of the authors and should not be interpreted as necessarily representing official policies or endorsements, either expressed or implied, of ARPA-H, DARPA, or the US government. J.C. is supported by the Natural Science and Engineering Research Council of Canada Postgraduate Scholarship-Doctoral. Y.C. is supported by the K. Lisa Yang Brain-Body Center Fellowship. S.O. is supported by the NIH through NIDDK 1F32DK139701-01 and NIDDK T32DK135449. **Author contributions:** J.C., A.A., and G.T. conceptualized the project. J.C., A.A., A.S., I.B., I.M., V.P., Y.C., Z.Y., and B.M. developed the electrical design. J.C., A.A, and A.S. developed the mechanical design. J.C., N.F., A.P., K.S., A.H., A.G., and B.L. designed and performed the animal studies. J.C., C.R., and N.S. developed the pH-activation mechanism. J.C., A.A., and A.S. performed the data processing and analysis. J.C., A.A., and G.T. conceptualized the project. J.C., A.A., A.S., I.B., I.M., V.P., Y.C., Z.Y., and B.M. developed the electrical design. J.C., A.A, and A.S. developed the mechanical design. J.C., N.F., A.P., K.S., A.H., A.G., and B.L. designed and performed the animal studies. J.C., C.R., and N.S. developed the pH-activation mechanism. J.C., A.A., and A.S. performed the data processing and analysis. All authors contributed to the writing of the manuscript. **Competing interests:** G.T. has no competing interests that are directly relevant. A full list of competing interests is available at www.dropbox.com/sh/szi7vnr4a2ajb56/AABs5N5i0q9AfT1IqIJAE-T5a?dl=0. All other authors declare that they have no competing interests. **Data and materials availability:** All data needed to support the conclusions of this manuscript are included in the main text or Supplementary Materials.

Submitted 1 March 2025
Accepted 24 September 2025
Published 22 October 2025
10.1126/scirobotics.adx1367

Science Robotics

An ingestible capsule for luminance-based diagnosis of mesenteric ischemia

J. Chen, A. Alexiev, A. Sergnese, N. Fabian, A. Pettinari, Y. Cai, V. Perepelook, K. Schmidt, A. Hayward, A. Guevara, B. Laidlaw, I. Moon, B. Markowitz, I. Ballinger, Z. Yang, C. Rosen, N. Shalabi, S. Owyang, and G. Traverso

Sci. Robot. **10** (107), eadx1367. DOI: 10.1126/scirobotics.adx1367

Science Robotics (ISSN 2470-9476) is published by the American Association for the Advancement of Science. 1200 New York Avenue NW, Washington, DC 20005. The title *Science Robotics* is a registered trademark of AAAS.